CHAPTER-6

Study of bioactivity of ZrO_2 substituted

1393-B3 Borate glass

6.1 Introduction

It is believed that German glass manufacturer Otto Schott first used borates in glass in the late 19th century. The human body provokes a response of tissue rejection against metallic and synthetic polymeric materials due to their composition, which differs from that of live tissues. This response manifests in the formation of scar tissue. Bone comprises a hydrated calcium phosphate compound known as hydroxyl carbonate apatite (HCA). Consequently, if a substance can generate an HCA layer inside the body, it will likely be well-tolerated and not provoke rejection [1]. Numerous studies have been conducted on bioactive glasses due to their ability to establish interfacial contact with host tissue by forming a HCA layer upon implantation [2–4]. Bioceramics are often used in orthopaedics, where the materials' biocompatibility and mechanical characteristics are very important [5]. Due to their remarkable property, these biomaterials have been used in various medicinal uses, including bone regeneration materials [6,7] and dentistry [8]. Initially, boron neutrons were used for cancer treatment [9]. After that, boron's chemistry is examined to determine its effect on human health. The conclusion that can be drawn from this is that boron is most likely combined with hydroxylated molecules in biological systems and that the reduction and activation of coenzymes and enzymes are essential components of its mechanism of action [10]. Borate glass has wide applications in the industrial and scientific field [11]. Subsequently, transition metal substituted glasses have emerged as a viable and promising substitute for borate bioactive bioglass. The presence of transition metal ions enhances the formation of an HCA layer on the material's surface when it comes into contact with physiological fluids. This layer is made of the same minerals as real bone, so it can bond better and faster with the organs around it. As a result, it accelerates the healing process and makes it easier for the implant and its surrounding tissues to work together. The modification of glass composition can probably control the speed at which the human body undergoes deterioration. This may be achieved by including materials

that can either accelerate or block the dissolution process, depending on the specific purpose for which the glass is designed. As an example, the oxides CoO [13], CuO [14-15], SrO [16], TiO_2 [17] and ZnO [18] have been seen to enhance bioactivity by increasing cell proliferation. Zirconium dioxide (ZrO_2) was included as a supplementary component in the composition due to its unique properties as an oxide ceramic substance, having better mechanical capabilities [18]. These features encompass elevated yield strength and fracture toughness [19,20]. Many studies have been done on ZrO_2 supplements in different glasses for application in the medical field [21-25]. This investigation focuses on the effects of ZrO_2 addition on several aspects, including crystallization, thermal properties, spectrum analysis, structural characteristics, and in vitro behaviours. Many research papers regarding infections due to orthopaedic metal implants are studied [26-28], and their replacement is found as bioglass samples to avoid these infections [29-30]. Therefore, they have been used in case of breast cancer treatment [31-32] and cell proliferation of the samples is studied on the osteosarcoma MG-63 cell line [33-37]. These results tell us whether these samples are suitable for orthopaedic implants or not. Characterization of 1393 bioactive glass substituted with ZrO_2 was studied [38]. In order to achieve the desired outcome at a lower melting temperature, silica was substituted with boric oxide in 1393 glass forming 1393B3 glass, this results in an energy-saving and more cost-effective bioactive glass.

Thus, the current study aims to synthesize bioactive glasses at low temperatures with improved mechanical strength and bone compatibility qualities appropriate for orthopaedic applications.

6.2 Materials and Methods:

6.2.1 Glass samples synthesis: The glasses under investigation were prepared in the form of batches of samples shown in Table 6.1. The preparation process was conducted using the usual melt-quenching method. Hence, the precursor substances H_3BO_3, Na_2CO_3, $CaCO_3$, K_2CO_3,

$MgCO_3$, ZrO_2 and P_2O_5 with 99.5 % purity were purchased from Loba Chemie Pvt Ltd. These were thoroughly weighed out and combined in stoichiometric ratios using an agate mortar to assess their uniformity. They were melted inside a platinum crucible to eliminate the volatile compounds H_2O, and CO_2 from the mixes. They were heated in an electric furnace at a rate of 5ºC per minute and melted at a temperature of 1200°C for 2 hours. Finally, the melts were rapidly quenched into distilled water [39]. Then, they dried in airy oven at 100°C. The obtained small lumps are crushed in a ball-mill machine.

Table 6.1 Chemical composition of the BZ sample (wt %).

Chemicals	**Base**	**BZ1**	**BZ2**	**BZ3**	**BZ4**
B_2O_3	53	52	51.5	51	50.5
CaO	20	20	20	20	20
Na_2O	6	6	6	6	6
P_2O_5	4	4	4	4	4
MgO	5	5	5	5	5
K_2O	12	12	12	12	12
ZrO_2	0	1	1.5	2	2.5

6.2.2 Physico-chemical, thermal and mechanical properties:

6.2.2.1 Physio-chemical properties:

To determine the density of these bioactive glasses, fine granular powder was subjected to uniaxial pressing using a hydraulic press at a pressure of 10 tons for a duration of 90 seconds. This process resulted in the formation of a green sample with dimensions of 10×2 mm^2. The green samples were heated up to 500 ºC in an electric furnace, characterized by a heating and cooling rate of 2˚/min. The Archimedes principle has been used to estimate the density of samples. Pallets that had been sintered were first dried at 70°C. Using diethyl phthalate as an

immersing liquid, three samples of each sample were tested, and the density was calculated using equation 6.1.

$$\rho = \frac{w_a}{\omega_a - \omega_b}\rho_b \quad \text{.....(6.1)}$$

Where ρ_b =density of buoyant, w_a = weight of the sample in air, w_b = weight of the sample in buoyant.

pH analysis: EI Alpha 01 Digital pH Metre was used to evaluate the pH value of the SBF-immersed bioactive borate glass samples at room temperature. Initially, the pH value of the SBF was maintained at 7.4 then the pH value of the SBF was measured at 1, 7, 14, 21, and 28 days intervals, respectively.

6.2.2.2 Thermal properties:

The glass transition temperature of BZ samples and the appropriate temperatures for isothermal treatments of glasses were determined using differential scanning calorimetry (DSC). Thermo-gravimetric Analysis (TGA) quantifies the mass of a sample while subjecting it to heating, cooling, or maintaining it at a constant temperature. In this experiment, we assessed the heat flow and weight loss of the borate bioactive samples by subjecting them to heating. Prior to testing, the materials were pulverized using an agate mortar and pestle for a duration of 20 minutes. A TG-DSC thermal analyzer from Mettler Toledo in Germany was utilized to collect DSC and TGA curves inside a temperature range of ambient temperature to 700 ºC. The heating rate employed was 10°/min. The technique utilized a nitrogen gas environment to ascertain the calcination temperature.

6.2.2.3 Mechanical properties:

Flexural strength and compressive strength are measured with the help of an Instron Universal Testing Machine (AGS 10Knd, SHIMADZU), a Tinius Olsen H10KL machine

having a full-scale load of 2500kg. The pallets were prepared. The pallet underwent a two-step heat treatment with a heating and cooling rate of 2◦/min. To obtain better pallets, the green body was heated up to 500°C, then, it cooled down to room temperature.

A compressive test utilizing UTM with a crosshead speed of 0.5 mm/min was conducted on cylindrical materials with dimensions of 10×9 mm^2. For every composition, three duplicates were chosen, and their values were averaged. Equation (2) was used to compute the BZ sample compressive strength. It was calculated with the following equation:

$$\textbf{Compressive strength (MPa)} = \frac{\mathbf{F}}{\pi \mathbf{r^2}} \quad \textbf{……..(6.2)}$$

Here, F= load in Newton, r=radius of the pallet

The flexural strength of a material is often described as the highest amount of bending stress that may be given to the material before it undergoes mechanical deformation. Equation 3 was utilized to evaluate BZ sample's flexural strength

$$\textbf{Flexural strength (MPa)} = \frac{3\times F\times l}{2\times b\times h^2} \textbf{……..(6.3)}$$

Where, F=load in Newton, l=length b=width h =thickness of the pallet

6.2.3 *In-vitro* characterization:

A standard procedure created by Kokubo et al [40] is used to make SBF in polypropylene bottles. The in vitro bioactive properties of the samples were investigated using the previously reported technique. 60 mg of each glass sample was submerged in 60 ml of SBF solution inside covered containers. These flasks were then put in an incubator set at a consistent temperature of 37°C. The samples were filtered and afterwards subjected to drying in an oven at a temperature of 70°C. The surface variations were investigated using X-ray diffraction (XRD), Fourier-transform infrared spectroscopy (FTIR), and SEM (Scanning electron microscope) - EDS (Energy dispersive X-ray spectroscopy):

6.2.3.1 FTIR spectroscopy analysis:

The spectral data of the formation of different bonds was collected at room temperature within the range of (400-4000 cm^{-1}) using a SHIMADZU IRAffinity-1S spectrometer with KBr medium.

6.2.3.2 XRD analysis:

The XRD patterns of the BZ samples were obtained using a Rigaku Miniflex 600 Desktop X-Ray Diffraction system was connected with a Cu anticathode, which is emitted Cu Kα radiation with a wavelength of 1.54056 Å. The measurements were conducted at room temperature. The experiments used the Bragg-Brentano geometry, with a scanning angle (2θ) increment of 0.05° throughout the 10–80° (step time = 2 sec, and step size = 0.02°).

6.2.3.3 SEM-EDS:

The bioactive glass sample's elemental content and surface morphologies were analyzed using a scanning electron microscope connected with an energy-dispersive X-ray spectrometer (SEM-EDS) (Nova Nano SEM 450, U.S.A.).

6.2.4 *In-vitro* hemocompatibility:

The *in-vitro* haemolysis study was done using a procedure that was already known [41]. In short, fresh blood from male Wister rats was taken from the retro-orbital vein and put in heparin-coated (anticoagulant) tubes. The tubes were then spun at 650 g for 10 minutes at 4ºC, and the supernatant was carefully thrown away. After washing RBC pellets using cold PBS until the supernatant was clear, blood was diluted in PBS solution with a ratio of 1:10 (blood: PBS). The resulting RBC culture (0.1 ml) was combined with various products (0.9 ml) at a rate of 1 mg/ml (in PBS). Triton x-100 represented as positive control (100 % lysis), and the blank PBS (pH 7.4) as negative control (no lysis) were used. These combined products were

placed in a shaker incubator at constant speed maintained at 37 ± 1 °C for 1 hr. Then, non-lysed red blood cells were separated from these combined products, centrifuging them at 650 g for 10 minutes maintained at 4ºC. With the help of a microplate reader, the supernatant's lysis was calculated by measuring the optical density at 540 nm.

$$\textbf{Hemolysis} = \frac{\textbf{Odsample} - \textbf{Od0}}{\textbf{Od100} - \textbf{Od0}} \textbf{ X 100}$$

(Od sample = optical density of sample, Od 0 = optical density of PBS and optical density of Triton-X)

6.2.5 Cellular compatibility:

MG-63 cell line (osteosarcoma) was purchased from NCCS Pune (India). Twelve well cell culture plates and DMEM (Dulbecco's Modified Eagle Medium) have been purchased from Genetics (Genetics Biotech Asia Pvt. Ltd). Eppendorf was the source of the T-25 flasks and 96 well plates. The reagents used in this study, namely Fetal Bovine Serum (FBS), penicillin-streptomycin and Trypsin-EDTA, were acquired from Gibco. Phosphate Buffer Saline (PBS) was manufactured using analytical-grade chemicals sourced from a highly reputable company. MG-63 cell line was subjected to incubation inside a controlled environment. This incubator environment is maintained at a temperature of 37 °C, having humidified CO_2. The cells were grown in DMEM, and FBS (Fetal Bovine Serum) was added to it. A penicillin-streptomycin solution was included to prevent the culture from getting contaminated by microorganisms and to keep the purity of the culture. This well-controlled environment and nutrient-rich media help MG-63 cells grow and proliferate. ZrO_2-substituted borate glass samples (Base, 1%, 1.5%, 2%, and 2.5%) were tested for MG-63 cell line growth using MTT assay. Ten thousand cells were planted in each 96-cell culture plate and left to heed overnight. ZrO_2 substituted bioactive borate glass samples were kept at 5 mg/ml in 1 ml PBS. After exposing to different concentrations (100µg/ml, 200µg/ml, 400µg/ml, 600µg/ml, 800µg/ml),

the cells were incubated for 24 hours. After removing DMEM from each well, an MTT-carrying medium was added. Following an incubation period of 2 hours, the medium containing the MTT was discarded, and 100 µl of DMSO was added to each well. Then after, the wells were incubated for 30 more minutes. Multiplate readers measured absorbance at 570 nm. Phase contrast Imaging of cell proliferation at regular intervals is obtained through a microscope (EVOS FL cell imaging system, Life Technologies, USA) at 100x magnification.

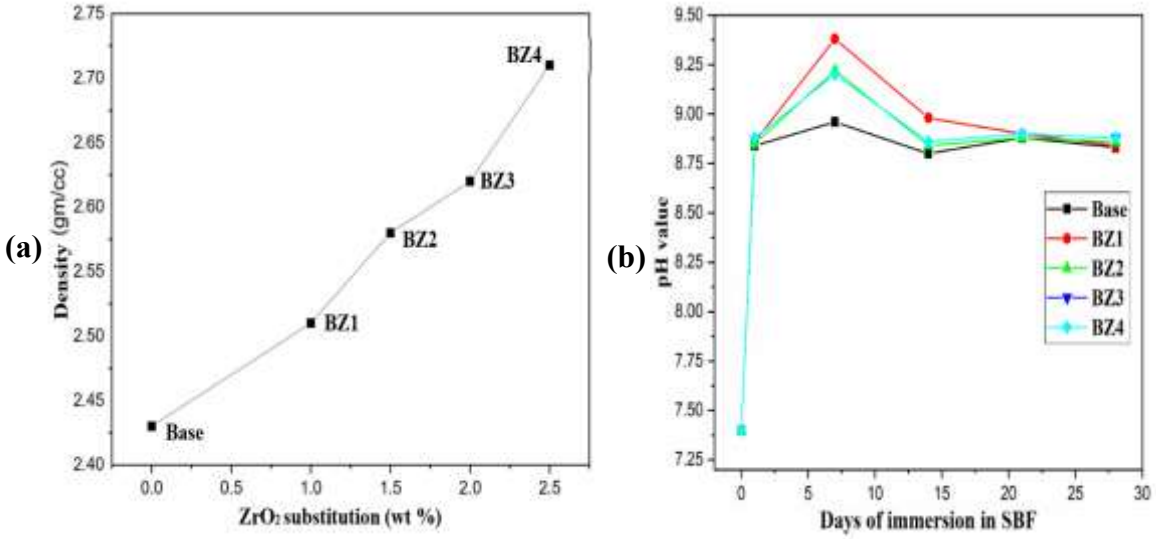

Figure 6.1 (a) Variation of density with increasing content of ZrO_2 in 1393-B3 Borate glass. **(b)** The pH value of SBF varies with the amount of days that BZ samples are submerged in it.

6.3 Results and Discussion:

6.3.1 Physico-chemical, thermal, and mechanical property analysis:

6.3.1.1 Physico-chemical properties:

The samples density was measured using formula 6.1a. As shown in Figure 6.1a, the density value increases as the content of ZrO_2 substitution increases in the 1393-B3 samples. The reason behind the increase in density value is that ZrO_2 density is more as compared to boric oxide. Increased density value increasing compactness of the samples are more suitable for its orthopaedic implant.

pH analysis: Figure 6.1b shows the pH changes of 1393-B3 borate bioactive samples substituted with ZrO_2 were submerged in SBF with different time interval. SBF-soaked sample

solution pH was increased, as shown in Figure 6.1b, which shows the leaching of alkali ions in the sample after SBF reactions. The observed result may be due to the rise in alkali ions (Na^{+}, Ca^{2+}, Mg^{2+}) concentration in the SBF due to bioactive glass dissolution [41]. This fluctuation suggests that the glass surface and biological medium exchange ions, facilitating HCA layer development. Ion motions promote HCA formation, raising pH over seven days, then after that, decreasing. After the HCA layer formation, ions mobility decreases, lowering the value of pH. Figure 6.1b shows this drop continues until it stabilizes after 28 days.

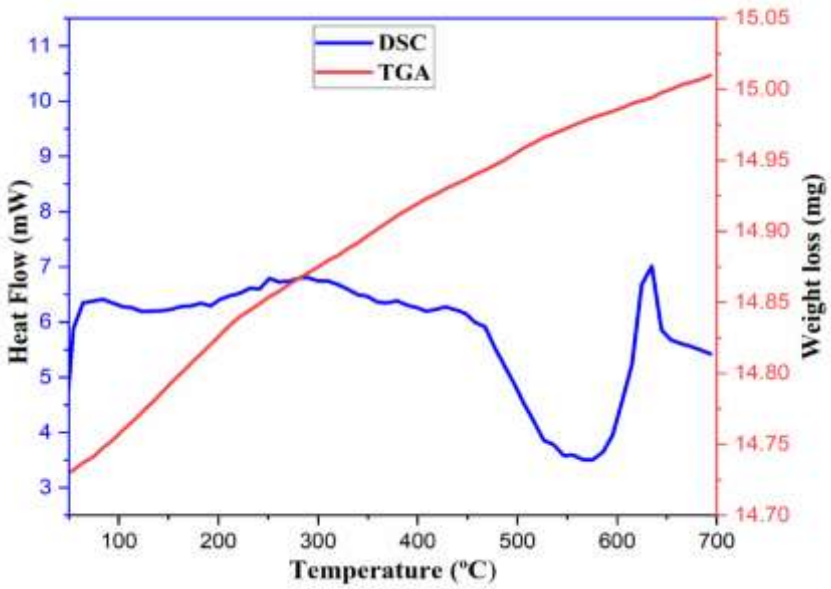

Figure 6.2.1 DSC /TGA analysis of base 1393-B3 borate glass.

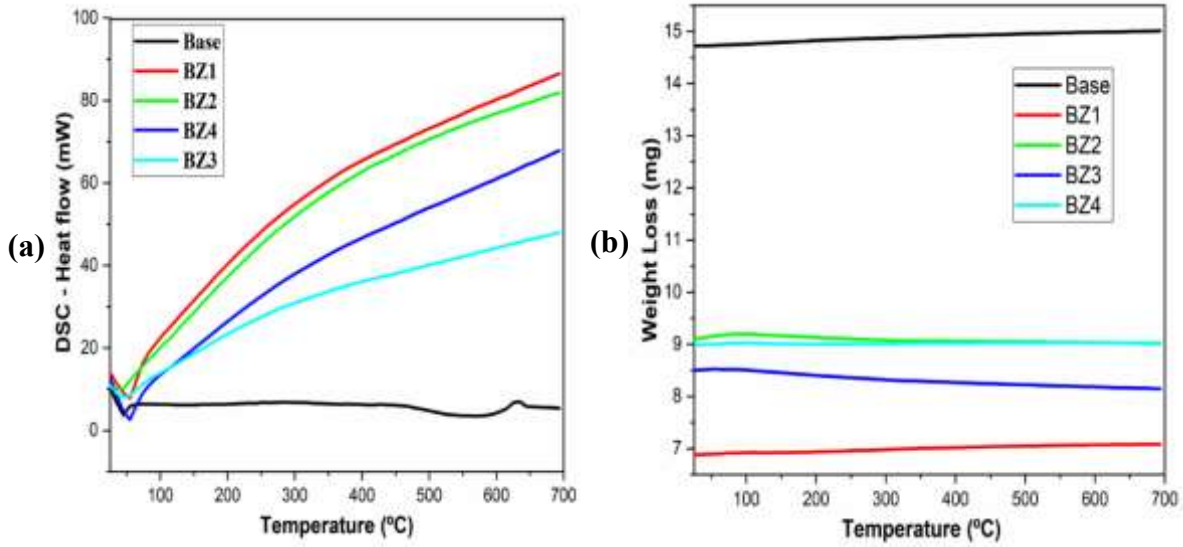

Figure 6.2.2 (a) DSC and **(b)**TGA graph of base and different wt% of ZrO_2 substitution in 1393-B3 borate glass.

6.3.1.2 Thermal properties:

The DSC study of base 1393-B3 borate glass sample indicated a glass transition temperature (Tg) of 467°C, a glass crystallization temperature (Tcr) of 635°C showing an exothermic event is consistent with the polymer chains breaks in the vulcanization process. (Figure 6.2.1). TGA analysis in Figure 6.2.1 shows the very low weight loss of the sample from 15.1 mg to 14.72 mg. The temperature range for DSC-TGA was set to 700 ºC, as some sample began melting after that. Figure 6.2.2a shows all sample DSC-heat flow graphs. This study found that replacing boric oxide with ZrO_2 increased heat flow, especially at higher temperatures [42]. In contrast, ZrO_2 melts at very high temperatures. A higher ZrO_2 content reduces heat flow. According to this the glass transition temperature is between 450-520 ºC, while the glass crystallization temperature is between 600-700 ºC. Figure 6.2.2b shows that TGA weight loss changes very little as the line becomes straight for a higher concentration of ZrO_2. Also, base 1393-B3 borate glass lost weight more at higher temperatures. The weight loss value for ZrO_2 replaced materials decreases as ZrO_2 content was increased in the sample. Since ZrO_2 substitution reduced weight loss, these data demonstrate better adaptation as it becomes more stable.

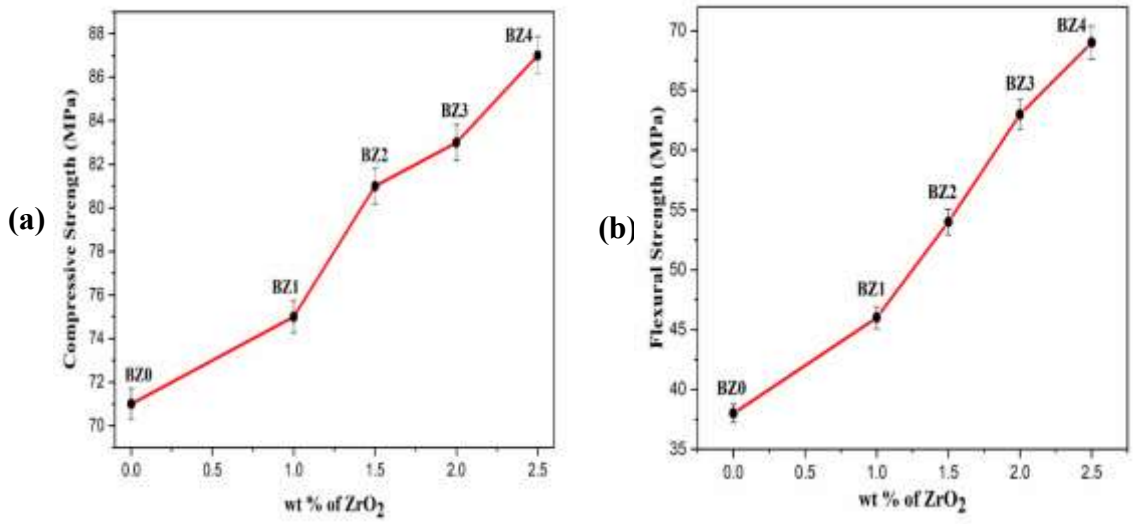

Figure 6.3 Mechanical properties variation of base and ZrO_2 substituted 1393-B3 glass samples **(a)** Compressive strength and **(b)** Flexural strength.

6.3.1.3 Mechanical properties:

The sample's compressive strength is calculated by equation 6.2, whereas its flexural strength is determined by equation 6.3. The flexural and compressive strengths of the samples were increased as the ZrO_2 substitution rises, as shown in Figure 6.3. These increased properties are beneficial when in contact with bone. Bone tissue connections become more robust and adaptable as samples expand. The main disadvantage of HCA is its mechanical properties, which are well recognized. Enhanced mechanical qualities may effectively decrease these restrictions.

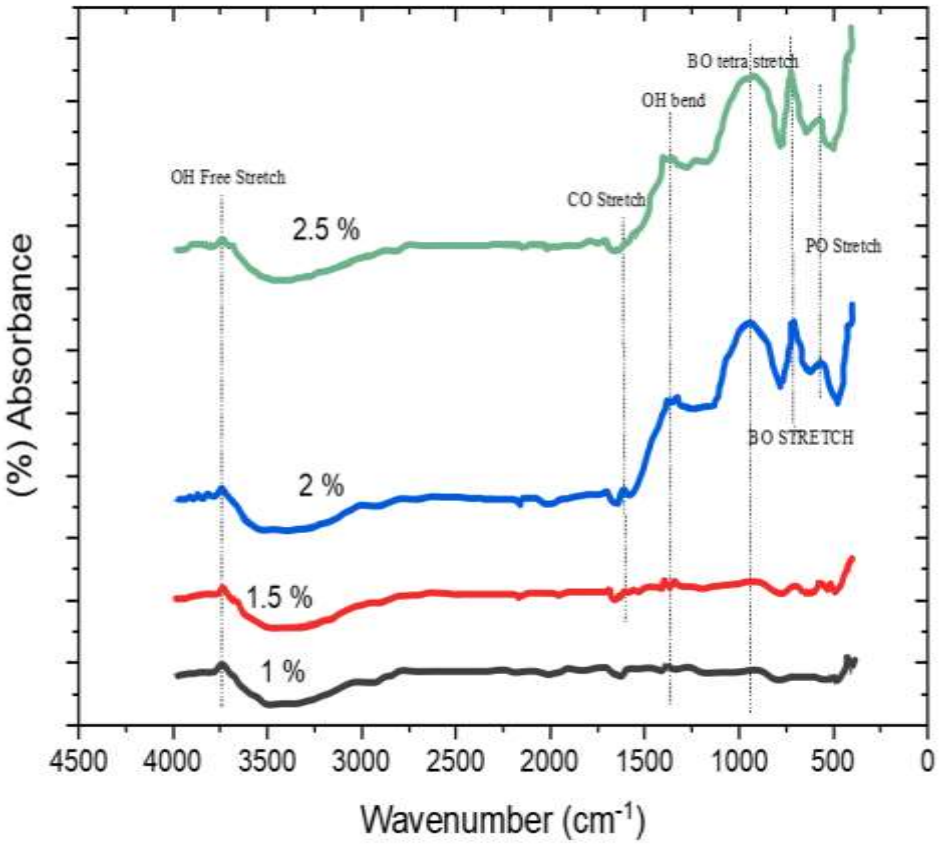

Figure 6.4.1 FTIR spectrum for different compositions of ZrO_2 substituted 1393-B3 borate glass before immersion in SBF.

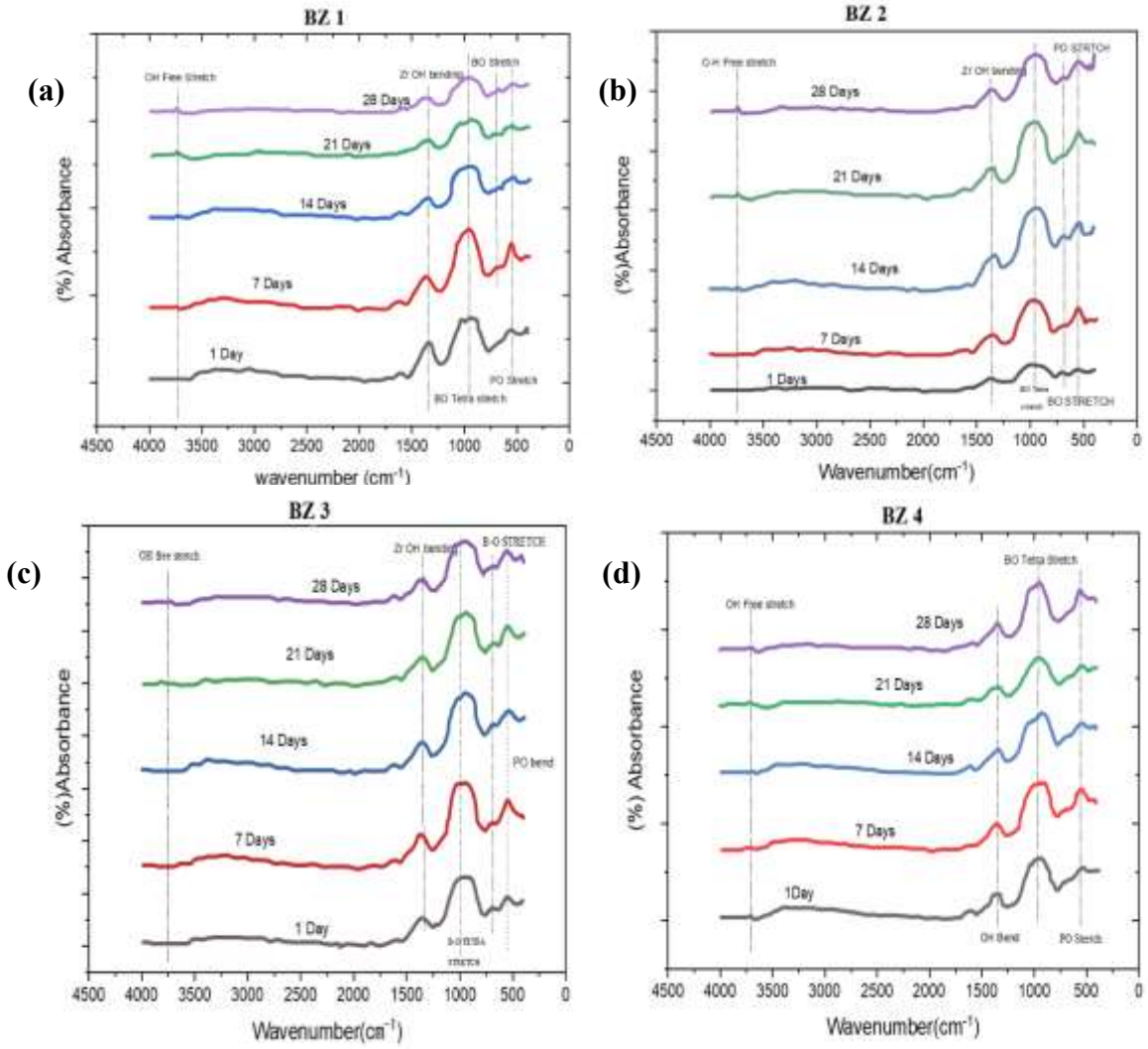

Figure 6.4.2 FTIR spectrum for BZ1(1%), BZ2(1.5%), BZ3(2%) and BZ4(2.5%) for different ZrO_2 substituted 1393-B3 borate glass after 1,7,15,21 and 28 days immersion in SBF.

6.3.2. *In-vitro* analysis:

6.3.2.1 FTIR analysis:

Figure 6.4.1 represents the base glass, which has only the prominent peaks of the hydroxyl group at the wavenumber of 3753 cm^{-1}, and there is no HCA layer formation which is confirmed by the absence of a phosphate bond. The presence of the HCA layer over the glass samples was mainly attributed to phosphate bonds, carbonyl, and hydroxyl groups. These linkages signify the creation of HCA bonds. In Figure 6.4.2, BZ1 sample shows the first peaks at wavenumber of 3745 to 3755 cm^{-1} which shows hydroxyl group (O-H stretch free). The second peak is shown at wavenumber of 1360 to 1380 cm^{-1} which indicates the presence of Zr-

OH bonding which is due to the dopant compound, the third peak is shown at the wavenumber of 1581 cm^{-1} which is of phosphate group presence, the fourth peak is at wavenumber 711 cm^{-1} showing the carbonate presence and finally at 553 cm^{-1}. In case of BZ2 sample the intensity of the bands has decreased corresponding to BZ1 showing the formation, the glass sample showed a new characteristic peak at wavenumber 592 cm^{-1}, which refers to P-O bending (crystalline) of HCA layer on it. In BZ3 sample the intensity of the bands is showing a decreasing trend with an increase in the time of the immersion; hence, it shows that with time, the HCA layer is forming suitably at its surface. In BZ4 represents substitution of the 2.5 wt% of ZrO_2 in 1393-B3 glass, i.e. borate based 1393 glass, in which the intensity of the bands is almost the same with all days of immersion [43]. Therefore, it is concluded that only HCA is present in all samples after SBF soaking. In this study, we look at how the formation of bond links leading to a hydroxyl apatite layer over the sample surface increases as the ZrO_2 substitution increases in the corresponding samples. Also, the bond peaks are sharper after the samples have been soaked in the SBF solution for a longer time, which is 28 days. So, these hydroxyl apatite bonds show an increase in the bioactivity of the samples as the ZrO_2 substitution increases in 1393-B3 borate samples.

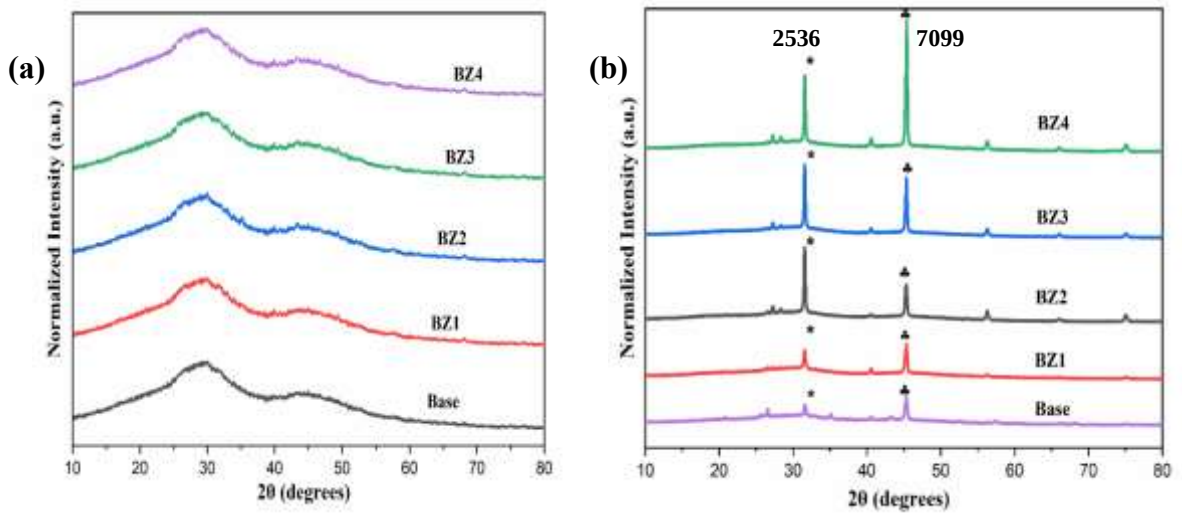

Figure 6.5.1 XRD graph of different wt % of ZrO_2 substitution in 1393-B3 borate glass **(a)** before SBF immersion and **(b)** after SBF immersion.

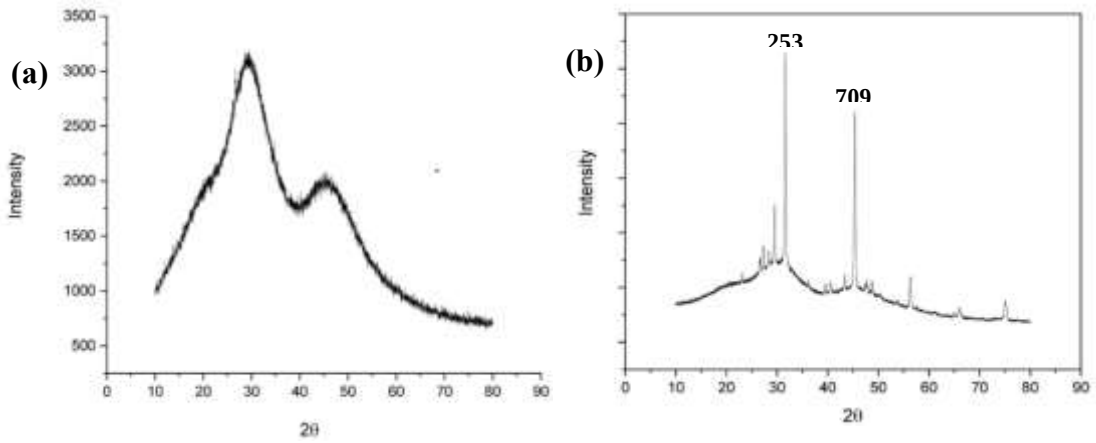

Figure 6.5.2 XRD graph of different 1.5 wt % of ZrO_2 (BZ2) substitution in 1393-B3 borate glass **(a)** before SBF immersion and **(b)** after SBF immersion.

6.3.2.2 Crystallographic Analysis:

The produced base and ZrO_2 substituted 1393-B3 bioactive glass samples were entirely amorphous, with no crystalline phase in any of the samples. In Figure 6.5.1a we observed that no sharp peak is present in the sample, while in Figure 6.5.1b, after soaking for 28 days, we found that sharp peaks are present in all the samples. Single XRD graph observation of BZ2 shown in Figure 6.5.2. Here Figure 6.5.2a shows no peak for the 1.5% ZrO_2 substituted 1393-B3 glass sample, while Figure 6.5.2b shows two sharp peaks. We arranged all the sample's results in the same graph in groups so that we could compare them easily. In Figure 6.5.1 X-ray diffraction pattern, it is seen that no distinct peaks were evident in any of the produced samples. It shows two different peaks in the samples after replacing ZrO_2 in 1393-B3 borate glass samples. A single distinct peak was seen at an angle of 31.7º (2θ), suggesting the existence of $Ca_{10.042}(PO_4)_{5.952}(OH)_{2.292}$ (JCPDS code-2536). Second steep peak is present at 45.3º (2 thetas) indicates the creation of a sodium phosphate bond, $Na_2(HPO)_4$ (code 7099), and this represents the phosphate bonds, as shown in JCPDS data analysis [44]. Sharp peaks are observed in the XRD pattern of 1393B3 borate glass samples containing varying wt % of ZrO_2 immersed in SBF solution for 28 days. The HA formation highest for BZ4.

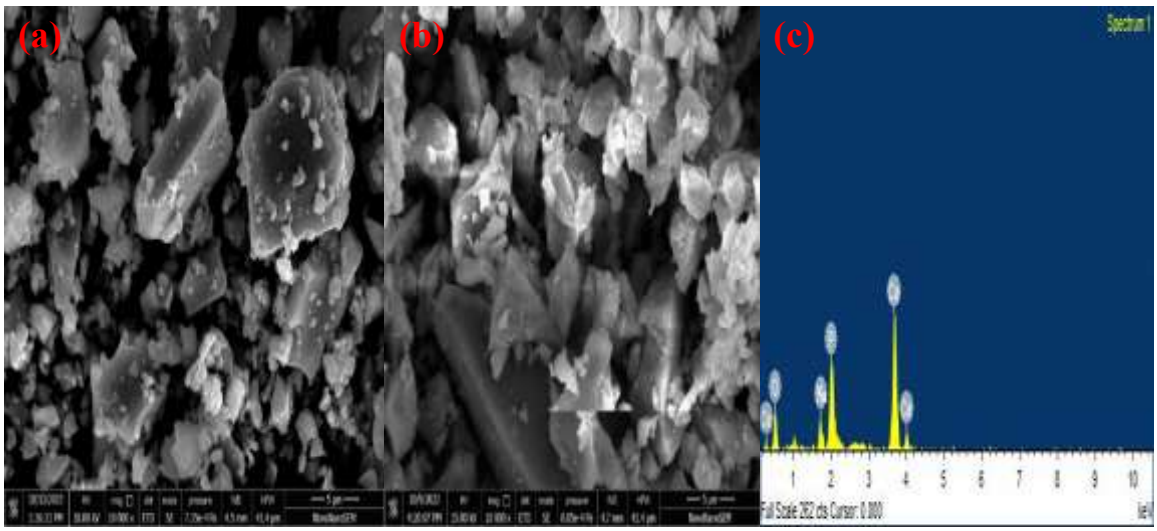

Figure 6.6.1 SEM image for Base 1393-B3 borate bioactive glass sample **(a)** SEM before SBF immersion **(b)** SEM after 28 days SBF immersion **(c)** EDS spectrum after 28 days SBF immersion.

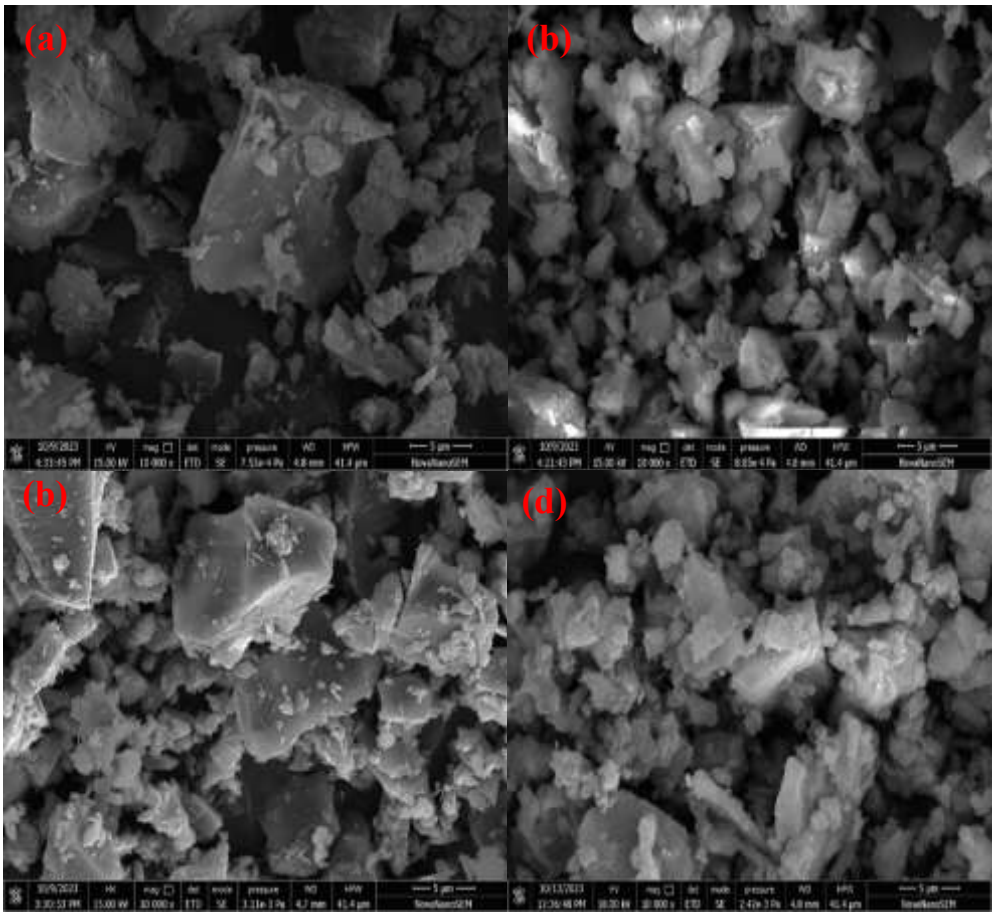

Figure 6.6.2 SEM images for 1 wt% ZrO_2 substituted 1393-B3 borate bioactive glass sample **(a)** before SBF immersion **(b)** after 28 days SBF immersion and for 1.5 wt% ZrO_2 substituted 1393-B3 borate bioactive glass sample **(c)** before SBF immersion **(d)** after 28 days SBF immersion.

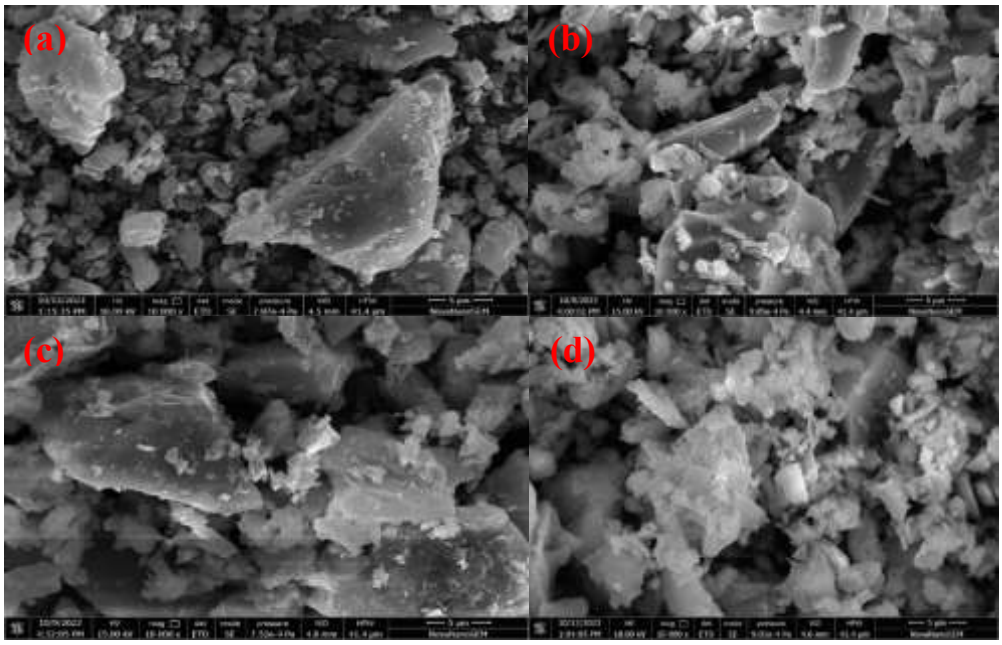

Figure 6.6.3 SEM images for 2 wt% ZrO_2 substituted 1393-B3 borate bioactive glass sample **(a)** before SBF immersion **(b)** after 28 days SBF immersion and SEM images for 2.5 wt% ZrO_2 substituted 1393-B3 borate bioactive glass sample **(c)** before SBF immersion **(d)** after 28 days SBF immersion.

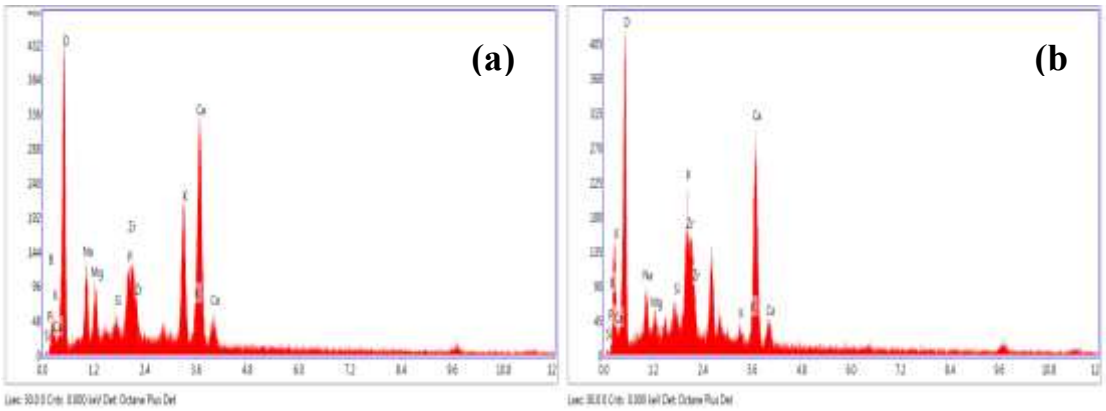

Figure 6.6.4 EDS spectrum image after 28 days SBF immersion for **(a)** 1.5 wt% ZrO_2 **(b)** 2.5 wt% ZrO_2 substituted 1393-B3 borate bioactive glass sample after SBF immersion.

6.3.2.3 Surface morphology and elemental analysis:

SEM images of the bioglass samples before in vitro study are observed and analyzed. Before the sample was SBF soaked, uneven surfaces made up of bits of different sizes with sharp edges and empty spaces between them were examined. The above micrographs were captured by SEM before and after immersing the prepared samples in SBF for a duration of 28 days. In these images, we observed that surface of the glass forming is a glassy structure.

The SEM images after they were put in the SBF show that some polycrystalline substance was being formed on the surface of the bioglass samples. This developed crystal layer on the surface is supposed to be the HCA layer. In Figure 6.6.1, the base 1393-B3 borate sample showed a thin layer of HCA over the sample after SBF immersion. In Figures 6.6.2 and 6.6.3, it has been observed that for increasing ZrO_2 content, the crystalline phase formed gets uniform shapes on the surface of the bioglass samples, and it has a needle-like structure. Thus, BZ samples produced a thick layer of HCA structures on their surfaces after SBF immersion. In Figures 6.6.1, 6.6.2, and 6.6.3, we found that maximum HCA layer formed for the 2.5 wt% of ZrO_2 substituted 1393-B3 borate bioactive glass sample.

Figure 6.6.4 shows the EDS spectrum of the sample after SBF immersion of BZ2 and BZ4 for 28 days. Here, observed that 2.5% wt% of ZrO_2 substituted 1393-B3 borate bioactive glass sample also approved the increase in the calcium and phosphorous content after SBF immersion [35,44]. This also confirms that maximum HCA layer formation for 2.5% ZrO_2 substituted 1393-B3 borate bioactive glass sample.

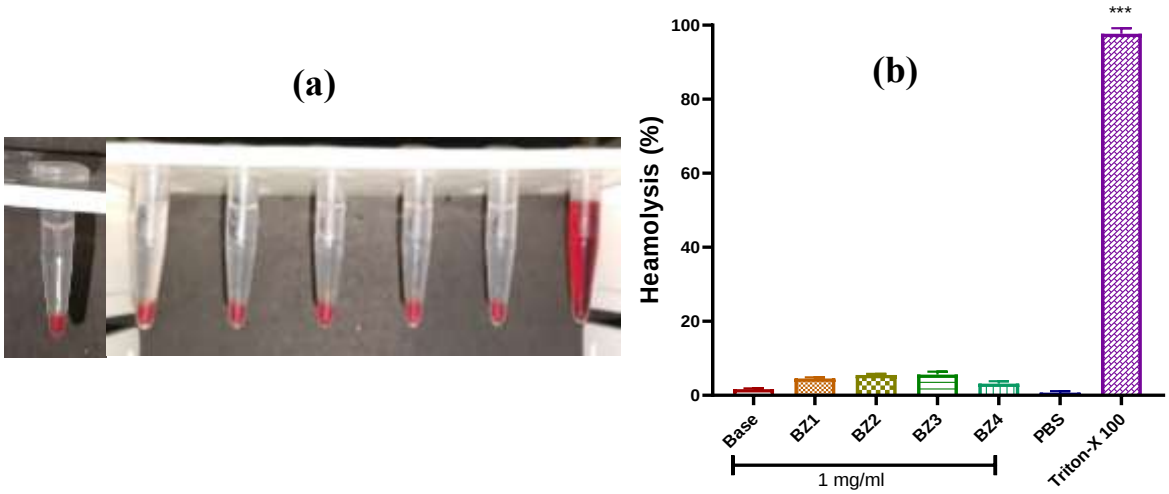

Figure 6.7 Ex vivo hemocompatibility of different wt% of ZrO_2 substituted 1393-B3 borate glass **(a)** represents the after haemolytic study, **(b)** % of hemolytic activity.

6.3.3 Hemocompatibility:

After performing the experiment, it was discovered that all of the BZ borate bioactive samples can be combined with human blood. No, it is impossible to lyse blood samples, as seen

in Figure 6.7(a). Because of this, we can assert that it is effective with human blood [48]. As seen in Figure 6.7(b), the products exhibited a hemolysis rate of less than 4%, which was significantly lower ($p < 0.01$) compared to the positive control group (triton x-100), which was known to have a powerful hemolytic impact [33]. Following the creation of these objects, it was discovered that they were compatible with blood and used for bone replacement.

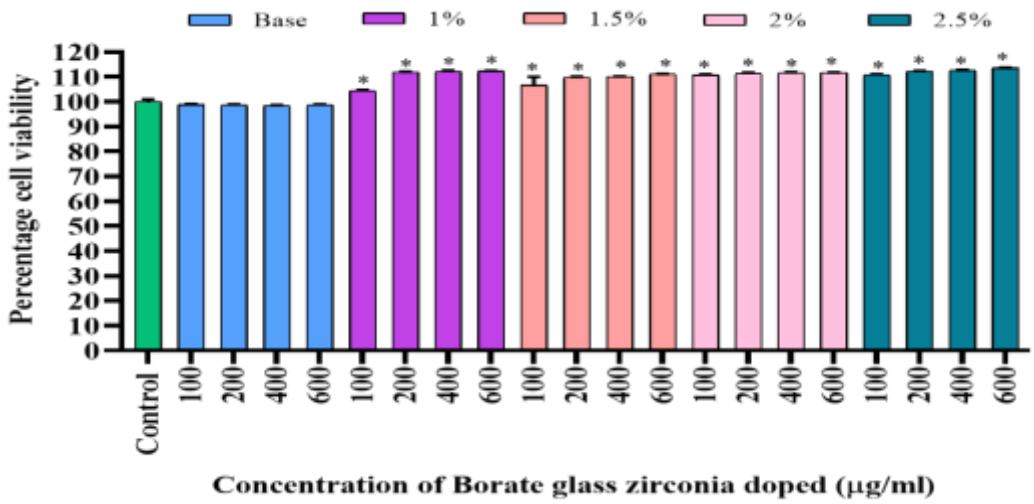

Figure 6.8.1 Bar diagram represents a cellular proliferation of titanium substituted with 1393-B3 borate glass sample against MG-63 cell line. Here * denotes a significant difference ($p<0.05$) compared to the control.

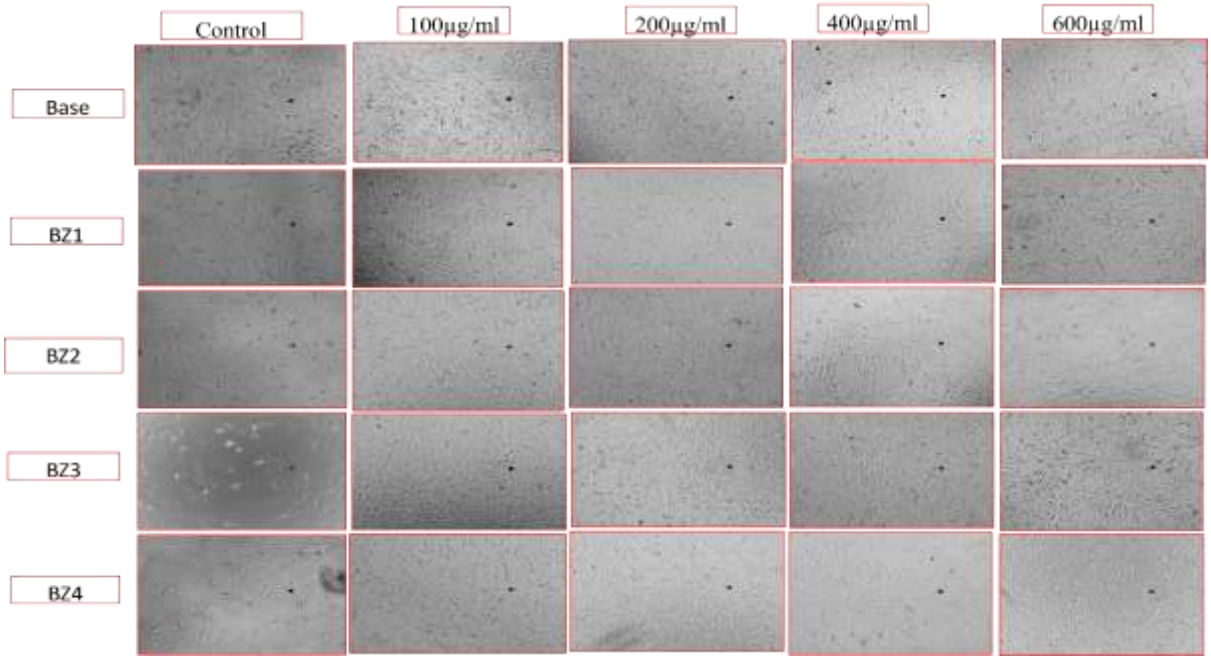

Figure 6.8.2 Phase contrast microscopic images (400µm) of ZrO_2 substituted 1393-B3 glass samples (Base, 1%, 1.5%, 2%, and 2.5%) against MG-63 cell lines at various concentrations (100, 200,400 and 600µg/ml) showing proliferation of cells in a concentration-dependent manner.

6.3.4 *In-vitro* cellular analysis:

6.3.4.1 Cellular compatibility assay:

The ZrO_2 substituted 1393-B3 borate glass samples (Base, 1%, 1.5%, 2% and 2.5%) induced concentration-dependent proliferation against MG-63 cells even at higher concentrations. In Figure 6.8.1, significant proliferation was seen in the treatment group as compared to the control group. Maximum proliferation was seen in 2.5 wt% of zirconia-substituted borate glass samples at 600µg/ml. Thus, the results suggested that zirconia substitution to 1393B3 borate glass samples significantly facilitates cellular viability and proliferation, indicating an exciting potential for bone regeneration.

6.3.4.2 Phase contrast Imaging:

In Figure 6.8.2, *in-vitro* cell imaging with phase contrast microscope data revealed that the proliferation of MG-63 cells was increases with increase in concentration of zirconia substitution to 1393-B3 borate glass samples. Cells were proliferated maximally in 2.5 wt% ZrO_2-substituted glass samples at the concentration of 600 µg/ml. This further validate the result of cellular compatibility assay. Thus, the present result demonstrates that ZrO_2-substituted 1393B3 borate glass samples have a remarkable potential for utilization in bone regeneration.

6.4 Summary:

The effect of the substitution of ZrO_2 on physico-chemical, mechanical, in-vitro bioactivity, hemocompatibility and cytocompatibility in 1393-B3 borate bioactive glasses was investigated. We found that increasing substitution of ZrO_2 percentages significantly improved the mechanical characteristics of samples, which is suitable, especially those related to bone replacement. The bioactivity of the BZ samples were enhanced after immersion in SBF for varying time periods. Bioactivity of the samples were observed by HCA layer

formation over the surface of BZ which was confirmed by FTIR, XRD and SEM-EDS techniques. Hemocompatibility was assessed by the degree to which it interacts with human blood, which shows it is compatible with human blood. Using the MG-63 osteosarcoma cell line, we found that cellular compatibility and phase contrast pictures indicate superior quality after ZrO_2 substitution increases. 1393-B3 glass samples showed improved biocompatibility with human bone tissues when ZrO_2 was substituted in the place of boric oxide relative to the primary sample. Therefore, it was concluded that the bioactivity of the BZ samples were increased as ZrO_2 replacement for B_2O_3 increased, and it is maximum for 2.5 wt% ZrO_2. Thus, the present investigation illustrates that BZ samples were found optimal for orthopaedic implants.

References:

[1] L.L. Hench, The story of Bioglass, J Mater Sci Mater Med. 17 (2006) 967–978.

[2] L.L. Hench, Bioactive materials: The potential for tissue regeneration, J. Biomed. Mater. Res. 21 (1998) 511–518.

[3] L.L. Hench, R.J. Splinter, W.C. Allen, Bonding Mechanisms at the Interface of Ceramic Prosthetic Materials, I. Biomed. Mater. Res. Symp. 2 (1971) 117–141.

[4] L. Hench, J. Polak, Third-Generation Biomedical Materials, Body Building: The B Ion. Hum. 295 (2002) 1014–1017.

[5] D. Shekhawat, A. Singh, M.K. Banerjee, T. Singh, A. Patnaik, Bioceramic composites for orthopaedic applications: A comprehensive review of mechanical, biological, and microstructural properties, Ceramics International 47 (2021) 3013–3030.

[6] L.L. Hench, N. Roki, M.B. Fenn, Bioactive glasses : Importance of structure and properties in bone regeneration, J. Mol. Struct. 1073 (2014) 24–30.

[7] L.L. Hench, J.R. Jones, Bioactive Glasses: Frontiers and Challenges, Frontiers in Bioengineering and Biotechnology 3 (2015) 1–12.

[8] G. Gheysen, P. Ducheyne, L.L. Hench, P. De Meester, Bioglass composites : a potential material for dental application, Bioma. 4 (1983) 81–84.

[9] R.F. Barth, A.H. Soloway, R.G. Fairchild, Boron Neutron Capture Therapy for Cancer, Scientific American 263 (1990) 100–107.

[10] V. Salih, K. Franks, M. James, G.W. Hastings, J.C. Knowles, I. Olsen, Development of soluble glasses for biomedical use Part II : The biological response of human osteoblast cell lines to phosphate-based soluble glasses, J. Mater. Sci. Mater. Med. II. 1 (2000) 615– 620.

[11] W.G. Woods, An introduction to boron: history, sources, uses, and chemistry. Environmental Health Perspectives 102 (1994) 5–11.

[12] M. Bengisu. Borate glasses for scientific and industrial applications: a review. Journal of Materials Science 51 (2016) 2199–2242.

[13] S.K. Yadav, V.K. Vyas, P. Anand, M.R. Majhi, R. Pyare, Destructive and non-destructive properties of cobalt oxide substituted 1393 bioactive glass**,** Rasayan Journal of Chemistry 10 (2017) 935-945.

[14] A. Ali, M. Ershad, V.K. Vyas, S.K. Hira, P.P. Manna, B.N. Singh, S.Yadav, P. Srivastava, S.P. Singh, R. Pyare, Studies on effect of CuO addition on mechanical properties and in vitro cytocompatibility in 1393 bioactive glass scaffold. Materials Science and Engineering: C 93 (2018) 341–355.

[15] B.M. Elmowafy, A. Abdelghany, R.M. Ramadan, R Ghazy, T. Meaz. Synthesis, structural characterization, and antibacterial studies of new borate 13-93B3 bioglasses with low copper dopant. Egyptian Journal of Chemistry, 65 (2022) 1–10.

[16] A. Ali, S.P. Singh, Ram Pyare, SrO assisted 1393 glass scaffold with enhanced biological compatibility. Journal of Non-Crystalline Solids 550 (2020) 120392.

[17] A.R. Ghazy, B.M. Elmowafy, A.M. Abdelghany, T.M. Meaz, R. Ghazy, R.M. Ramadan, Structural, optical, and cytotoxicity studies of laser irradiated ZnO doped borate bioactive glasses. Scientific Reports, 13 (2023) 1-12.

[18] R.C. Garvie, R.H. Hannink, R.T. Pascoe, Ceramic steel? Nature 254 (1975) 703–704.

[19] C. Piconi, G. Maccauro, Zirconia as a ceramic biomaterial, Biomaterials 20 (1999) 1–25.

[20] M. Ferraris, E. Verné, P. Appendino, C. Moisescu, A. Krajewski, A. Ravaglioli, A. Piancastelli, Coatings on zirconia for medical applications, Biomaterials 21 (2000) 765–773.

[21] R. Samudrala, G.V.N. Reddy, B. Manavathi, P.A. Azeem, Synthesis, Characterization and Cytocompatibility of ZrO2 Doped Borosilicate Bioglasses. Journal of Non-Crystalline Solids 447 (2016) 150-155.

[22] P. Yin, J.W. Yuan, L.H. Liu, T. Xiao, T. Lei, Effect of ZrO2 on the bioactivity properties of gel-derived CaO-P2O5-SiO2-SrO glasses. Ceramics International 43 (2017) 9691–9698.

[23] A. Moghanian, M. Zohourfazeli, M.H.M. Tajer, The effect of zirconium content on in vitro bioactivity, biological behavior and antibacterial activity of sol-gel derived 58S bioactive glass, Journal of Non-Crystalline Solids, 546 (2020) 120262.

[24] A.M. Bannunah, Biomedical Applications of Zirconia-Based Nanomaterials: Challenges and Future Perspectives, Molecules 28 (2023) 5428.

[25] T. Tosiriwatanapong, Weerachai Singhatanadgit, Zirconia-Based Biomaterials for Hard Tissue Reconstruction. Bone and Tissue Regeneration Insights, 9 (2018) 1-9.

[26] V. Kandi, S. Vadakedath, Implant-Associated Infections: A Review of the Safety of Cardiac Implants, Cureus 12 (2020) e12267.

[27] J.R. Lentino, Prosthetic joint infections: bane of orthopedists, challenge for infectious disease specialists, Clin. Infect. Dis. 36 (2003) 1157–1161.

[28] A. Ewald, S.K. Gluckermann, R. Thull, U. Gbureck, Antimicrobial titanium/silver PVD coatings on titanium, Biomed. Eng. Online 5 (2006) 22.

[29] P. Ducheyne, Q. Qiu, Bioactive ceramics: the effect of surface reactivity on bone formation and bone cell function. Biomaterials, 20 (1999) 2287–2303.

[30] I. Qayoom, A.K. Teotia, A. Panjla, S. Verma, A. Kumar, Local and sustained delivery of rifampicin from a bioactive ceramic carrier treats bone infection in rat tibia, ACS Infect. Dis. 13 (2020) 2938–2949.

[31] D.N. Kumar, A. Chaudhuri, F. Aqil, D. Dehari, R. Munagala, S. Singh, R.C. Gupta, A.K. Agrawal, Exosomes as Emerging Drug Delivery and Diagnostic Modality for Breast Cancer: Recent Advances in Isolation and Application. Cancers 14 (2022) 1435.

[32] V. Kushwah, S.S. Katiyar, C.P. Dora, A.K. Agrawal, D.A. Lamprou, R.C. Gupta, S. Jain, Co-delivery of docetaxel and gemcitabine by anacardic acid modified self-assembled albumin nanoparticles for effective breast cancer management. Acta Biomaterialia, 73 (2018) 424–436.

[33] N. Price, S.P. Bendall, C. Frondoza, R.H. Jinnah, D.S. Hungerford, Human osteoblast-like cells (MG63) proliferate on a bioactive glass surface. Journal of Biomedical Materials Research, 37 (1997) 394–400.

[34] S. Yadav, P. Singh, R. Pyare, Synthesis, characterization, mechanical and biological properties of biocomposite based on zirconia containing 1393 bioactive glass with hydroxyapatite. Ceramics International, 46 (2020) 10442–10451.

[35] A. Singh, P. Goswami, B. Koch, P. Singh, R. Pyare, Study of Human Osteosarcoma Cell Line Growth, Hemocompatibility, In-vitro Analysis and Physical Properties of V_2O_5 Substituted Borosilicate Glass, Silicon 16 (2024) 1876-9918

[36] S.K. Singh, Jitendra Kumar, Priya Singh, S.K. Rajput, Ashutosh K. Dubey, Ram Pyare, and P.K. Roy. "Impact of 13-93 Bio-glass Inclusion on the Machinability, In-vitro Degradation, and Biological Behavior of Y-TZP-based Bioceramic Composite." Ceramics International 50 (2023) 1087-1106.

[37] N. Mutlu, F. Kurtuldu, I. Unalan, Z. Neščáková, H. Kaňková, D. Galusková, M. Michálek, L. Liverani, D. Galusek, A.R. Boccaccini, Effect of Zn and Ga Doping on Bioactivity, Degradation, and Antibacterial Properties of Borate 1393-B3 Bioactive Glass, Ceramics International 48 (2022) 16404-16417.

[38] S.K. Yadav, V.K. Vyas, S. Ray, M. Ershad, A. Ali, S. Prasad, M.R. Majhi, R. Pyare, In vitro bioactivity and mechanical properties of zirconium dioxide doped 1393 bioactive glass, International Journal of Scientific & Engineering Research 8 (2017) 2229-5518.

[39] S.A.S.N. Fadzli, R. Shamsudin, S.R. Zainuddin, J. Banjuraizah, F. Zainuddin. Preparation and Characterization of Macroporous Bioactive Glass Ceramic made via Sol-Gel Route and Powder Sintering Method. Sains Malaysiana, 47 (2018) 1025–1031.

[40] T. Kokubo, H. Kushitani, S. Sakka, T. Kitsugi, T. Yamamuro, Solutions able to reproduce in vivo surface-structure changes in bioactive glass-ceramic A-W, Journal of Biomedical Materials Research, 24 (1990) 721–734.

[41] T. Kokubo, H. Takadama, How useful is SBF in predicting in vivo bone bioactivity ?, Biomaterials, 27 (2006) 2907–2915.

[42] J. Xia, Y. Xiong, S. Min, J. Li, A review of recent infrared spectroscopy research for paper, Applied Spectroscopy Reviews 58 (2022) 738-754.

[43] U. Kumar, D. Yadav, A. K. Thakur, K. K. Srivastav, S. Upadhyay, Investigation on phase formation of Sr2SnO4 and effect of La-doping on its structural and optical properties, Journal of Thermal Analysis and Calorimetry 135 (2019) 1987–1999.